Contents lists available at **SCCE**

Journal of Soft Computing in Civil Engineering

Investigating the Correlation between the Parameters of Ground Motion Intensity Measures for Iran's Data

Mansoureh Rezaeemanesh[1*] (iD), Mohammadreza Mashayekhi[2] (iD)

1. Ph.D. Student, School of Civil Engineering, College of Engineering, University of Tehran, Tehran, Iran
2. Assistant Professor, Department of Civil Engineering, K.N. Toosi University of Technology, Tehran, Iran

Corresponding author: *mrezaeemanesh@ut.ac.ir*

https://doi.org/10.22115/SCCE.2022.344135.1450

ARTICLE INFO

ABSTRACT

This paper presents a statistical correlation analysis of peak ground acceleration to peak ground velocity ratio (A/V) and other ground motion intensity measures (IMs) for Iran's data. A/V is an important parameter that can significantly affect nonlinear structural responses. Findings from this study provide beneficial insights into selecting suitable parameters for characterizing earthquake ground motions. The studied database included 2053 strong ground motion records with the moment magnitude from 4.5 to 7.8 MW, rupture distance from 1 to 600 km, and average shear wave velocity from 155 to 1594 m/s. Correlation coefficients between A/V and several IMs were obtained for near-field and far-field records at three A/V levels, low A/V, middle A/V, and high A/V. Regression analyses for predicting A/V from the IMs were also conducted for near-field and far-field records. The results showed that the mean period (Tm) has the highest correlation with A/V at all A/V levels and for both far-field and near-field earthquakes compared to the other IMs. Therefore, this parameter can be employed for record selection as a frequency content-based parameter. Finally, current results showed that the accuracy of the Artificial Neural Network (ANN) models are more than the regression models for predicting A/V.

1. Introduction

Iran is located in a highly active seismic zone that has experienced multiple devastating earthquakes such as Bam, Tabas, and Manjil earthquakes [1–3]. In that regard, designing structures that can reliably withstand earthquake ground motions is imperative. One major step in the seismic design of structures is to characterize earthquake ground motions that can occur in the building site. Three main characteristics of earthquake ground motions are intensity, frequency content, and duration. Several intensity measures (IMs) are available in the literature to reflect these characteristics [4]. The relationship between these IMs is an important factor in the appropriate selection of the ground motion record used for the seismic design of a given structure, which affects its dynamic analysis and assessment of behavior [5].

One proposed IM is the peak ground acceleration (PGA) to peak ground velocity (PGV) ratio (A/V). Previous research indicates that considerable differences in A/V could be expected due to different source distances, faulting processes, and local geological conditions. In terms of structural responses, this ratio reflects information regarding the significant frequency content of the input earthquake motions [6]. In structure's nonlinear time-history analyses, A/V has been used as an empirical parameter to estimate ground motion frequency content and categorize ground motion suites. Ground motions are usually classified into three ranges: low A/V, middle A/V, and high A/V to reflect low-, middle-, and high-frequency contents, respectively [7]. A/V used with PGA or PGV could present a much better measure of ground motion damage potential for a wide range of structures. Hence, A/V should be taken into account in seismic design load specification [8].

PGV and PGA are mostly regarded as the main ground motion IMs used to perform analysis of nonlinear time-history. PGV is scaled to construct the design response spectrum, used in several seismic design codes as the ground motion IM for all structure levels. Seismic investigations have shown that waves with high-frequency are related to PGA, whereas waves with intermediate or low frequencies are related to PGV [8]. Numerous studies, including [9–17], have been performed on ground motion intensity measures, indicating that the perusal of IMs, which reveals the power of an earthquake, has become an integral part of earthquake engineering, especially after the occurrence of many strong earthquakes such as the 1994 Northridge Earthquake.

The effect of A/V on structural damage has been investigated in many studies [18–24]. Zhu et al. represented earthquake ground motion in the high, normal, and low A/V ranges using three sets of real earthquake records and studied the effect of A/V on structural damage. They realized that the A/V range significantly affects peak inelastic response, hysteretic energy dissipation, and stiffness deterioration of stiffness degrading systems. They also found that the effect on hysteretic energy dissipation is more pronounced and greater than that on peak inelastic response [6]. In another work, Zhu et al. investigated the importance of A/V on the displacement ductility demand for simple bilinear hysteretic systems by performing a static analysis. They concluded that the A/V range has an important effect on the displacement ductility demand, and it must be accounted for in design strength specification [25]. Several studies have been performed to correlate A/V to various other seismic parameters. TSO et al. examined the engineering implication of A/V. They analyzed a set of seismic data that included 45 strong ground motion

records to study the importance of A/V as a parameter for representing the dynamic characteristics of seismic motions induced by different seismic environments. They concluded that A/V is a good measure for classifying ground motions with similar frequency contents to construct the design response spectrum shapes [8]. Sawada et al. investigated A/V in terms of spectral characteristics of ground motion and earthquake duration. It was found that A/V is a superior parameter to represent the spectral characteristics and the duration of seismic ground motions [26]. Rathje et al. stated in their research that it is useful to describe the frequency content of earthquake ground motion with a simple parameter in practical earthquake engineering. They estimated three simplified frequency content parameters: the mean period, the predominant period, and the smoothed predominant spectral period. They calculated these three parameters for 306 records of 20 earthquake events and used nonlinear regression analysis for this data to provide a model that describes the magnitude, distance, and site dependence of the three abovementioned frequency content parameters. They concluded that the mean period parameter is the best frequency content parameter and could be reliably estimated [27]. The frequency content of earthquake ground motion is crucial because it affects the dynamic response of the ground and the structural system. Rathje et al. presented four experimental relationships for four frequency content parameters: the smoothed predominant spectral period, the mean period, the predominant spectral period, and the average spectral period. As a general conclusion, they also stated that all these four parameters could be predicted with good accuracy. Nevertheless, they added that the mean period parameter is preferred because it best describes the frequency content of earthquake ground motions[28]. Bommer et al. investigated several effective cycles of earthquake ground motion and earthquake duration correlations [29]. Garg et al. did research around the ground motion frequency content and A/V correlation. They conducted a linear regression analysis of data obtained from three earthquakes and concluded that the A/V might be used as an empirical parameter to estimate only the mean frequency content of the earthquake ground motion. [7]. Tavakoli et al. investigated the different effects of seismic parameters in near - and far-fault earthquakes. They showed that the damages due to near-fault earthquake records represented by Arias intensity (AI) and cumulative absolute velocity (CAV) are more dangerous than those from far-field ones [30]. Some other studies have focused on producing artificial records, which can be utilized to study the effect of seismic parameters in the near-field and far-field [31]. Oliveira et al. conducted an overall analysis of seismic ground motion parameters such as Housner intensity (HI), AI, CAV, PGA, and PGV. Their general conclusion based on the ratios of soil amplification was that weak motion (low magnitudes and long distances) leads to larger amplification compared to strong motion (large magnitudes and short distances) [32]. Garg et al. investigated the relationship between various parameters of ground motion for the 1991 Uttarkash, 1988 Indo-Burma, and 1988 Indo-Bangladesh earthquake records. The regression analyses showed that A/V has a strong relationship with ground motion mean frequency content and a weak relationship with ground motion predominant frequency content [7]. Huang and Galasso investigated the ground motion IM correlations in Italian strong motion records, which they also utilized to develop a new ground motion model [33]. Elhout investigated the relationship between the ground motion IMs and PGA to PGV ratio, which can be useful for figuring out the behavior of structures. The results indicated that the mean period has the best correlation with PGA/PGV [15]. A/V depends on the epicentral distance of the site, magnitude, and predominant period. Naumoski et al. and

Tso et al. regarding A/V, divided the seismic ground motions into the low, high, and middle ranges. Accordingly, having PGV (m/s) and PGA (g) values, PGA/PGV<0.8 g/m/s represents a low range and $0.8\,\text{g/m/s} \leq \text{PGA/PGV} \leq 1.2\,\text{g/m/s}$ represents a middle range, and PGA/PGV>1.2 g/m/s is classified as the high limit [8,34]. According to previous research, it can be said that the correlation between the IMs of ground motion and A/V is useful in evaluating the behavior of structures.

In the present study, an investigation was conducted on the correlation of A/V and other ground motion IMs in Iranian strong motion records. In this regard, first, the records were divided into two categories of near- and far-field earthquakes. Then, the A/V of each record was obtained and was plotted against IM parameters such as average spectral acceleration ($S_{a,avg}$), impulsivity index (IP), predominant period (T_p), Arias intensity (AI), number of effective cycles (N_{cy}), A95 parameter, mean period (T_m), cumulative absolute velocity (CAV), and damage index (DI). Finally, the correlation of the above IMs was investigated by performing a Regression analysis. The use of Artificial Neural Networks is examined to develop the prediction equation for A/V.

2. Database

A total of 1744 far-fault ground motion records and 309 near-fault ground motion records were used in the analysis conducted in this study. The records belonged to the Iran Strong Motion Network (ISMN) [35], which were prepared in [36]. In addition, the dataset was updated until 2021. Figure 1 illustrates the map of seismicity in Iran as reported by ISMN, which was used in this research. In the literature, there are different views to determine the distance limit for the near- and far-field earthquakes, and a single number has not been specified for it. For example, Heydari and Mousavi, Bhandari et al., and Xiaogang Huang et al. respectively considered 60, 50, and 10 km as the distance limit for the near- and far-field earthquakes [37,38]. Also, several researchers considered 20 km as the distance limit for the near- and far-field earthquakes in their research [28,39–43]. In this research, the far-field records were selected from sites with more than 20 kilometers of distance, whereas the near-field records were selected from sites with less than 20 kilometers of distance. The considered earthquake records covered a broad range of frequency contents and ground motion durations. Also, their moment magnitude scale (Mw) ranged from 4.5 to 7.8 for different soil types. In addition, the rupture distance (R_{rup}) , defined as the slant distance to the closest point on the rupture plane, shown in Fig. 2, was prepared from the ISMN website. The minimum and maximum rupture distances considered were 1 and 600 km, respectively. Figures 3 and 4 show the distribution of the moment magnitude versus the rupture distance of the records used in this study for the near- and far-field earthquakes, respectively. Furthermore, Figs. 5 and 6 depict the soil shear wave velocity distribution in the top 30 m of depth with respect to the rupture distance for the near- and far-field data, respectively. The minimum and maximum values for the soil shear wave velocity in the top 30 m of earth depth were 155 and 1594 m/s, respectively. The A/V values also ranged from 0.12 to 2.5 for the near-fault records and from 0.08 to 2.22 for the far-fault records.

The characteristics of some of the near- and far-field records considered are given in Tables 1 and 2, respectively. The 2053 records selected were categorized into three groups based on their A/V values, where A denotes the peak ground acceleration in terms of the gravitational

acceleration (g), and V denotes the peak velocity in m/s. Records with 0.8 g/m/s > PGA/PGV were categorized as the low A/V range, and records with PGA/PGV > 1.2 g/m/s were categorized as the high A/V range. Also, records with $0.8 \, \text{g/m/s} \leq \text{PGA/PGV} \leq 1.2 \, \text{g/m/s}$ represented the middle A/V range. Figure 7 illustrates the peak ground acceleration versus peak ground velocity diagrams for the near- and far-field records categorized into the low, middle, and high A/V groups.

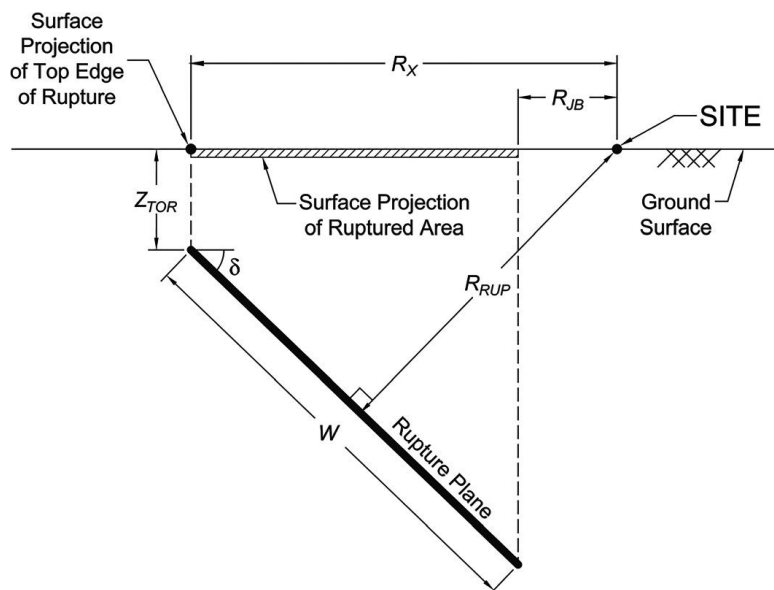**Fig. 1.** Map of seismicity in Iran as reported by the ISMN [35].

Fig. 2. Vertical cross-section of a fault rupture plane illustrating the earthquake source and distance measurements [44].
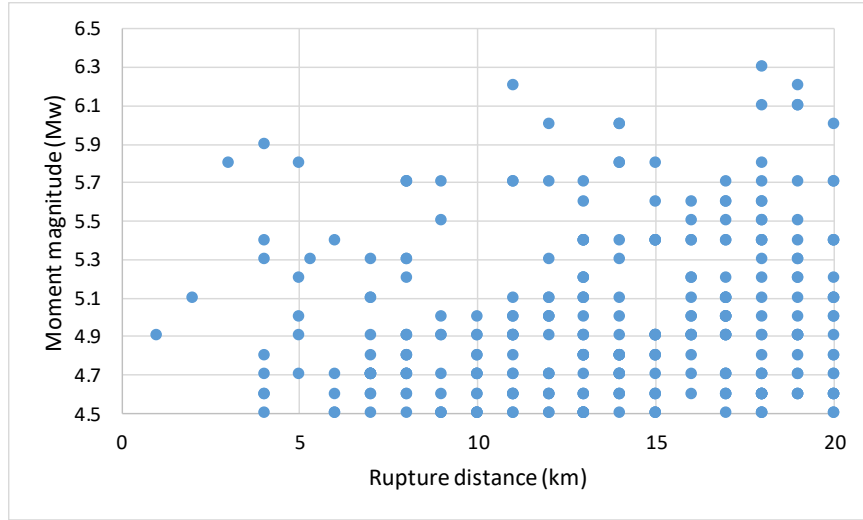
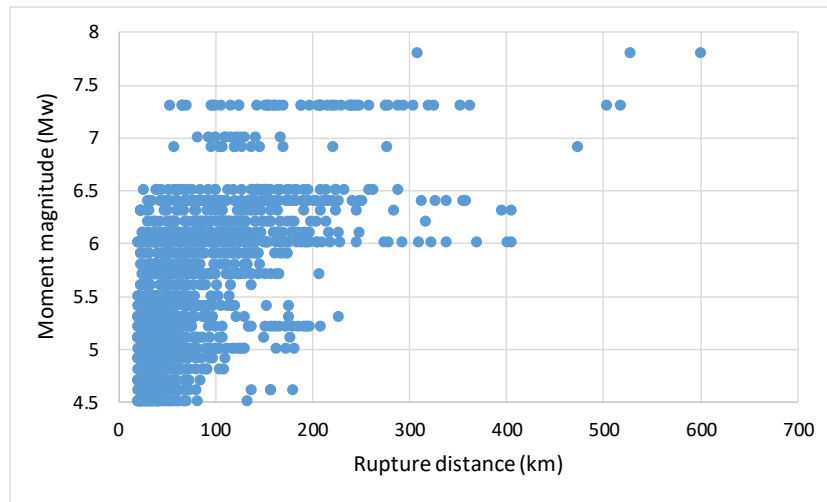**Fig. 3.** Distribution of the near-field records used in this study.

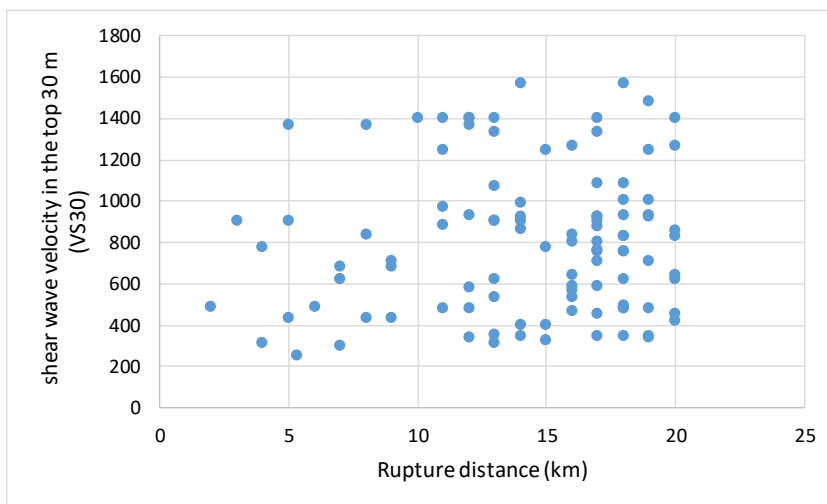**Fig. 4.** Distribution of the far-field records used in this study.

Fig. 5. Distribution of soil shear velocity in the top 30 m depth versus rupture distance for the near-field data.
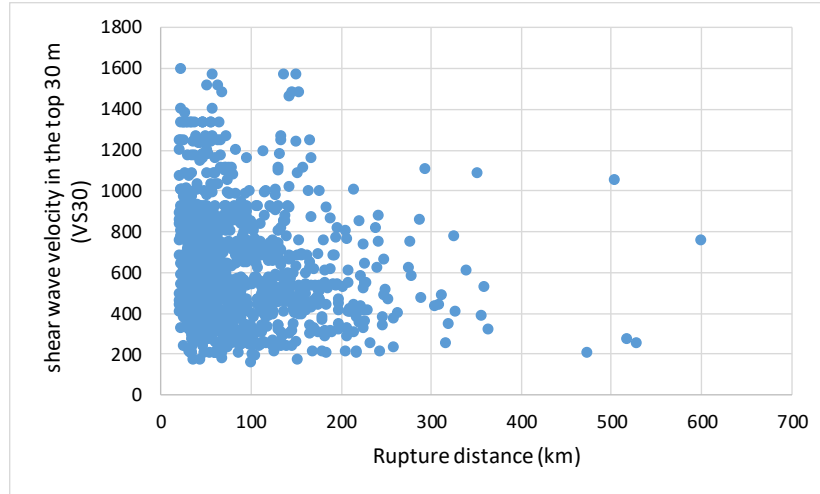
Fig. 6. Distribution of soil shear velocity in the top 30 m depth versus rupture distance for the far-field data.
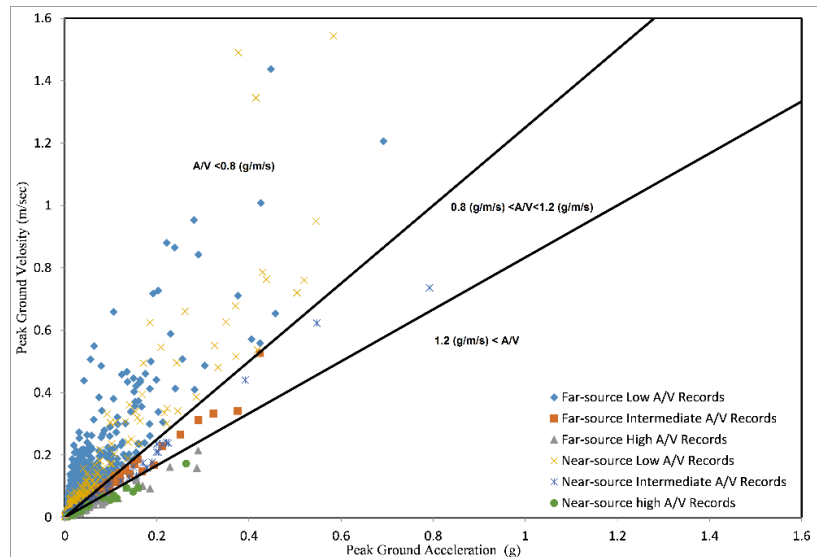
Table 1
Characteristics of some of the near-field records used in this study.

A/V Range	Record ID	Station Name	Lat.	Long.	R_{rup} (km)	Mw	$V_{S(30)}$ (m/s)	PGA (g)	PGV (m/sec)	PGD (m)	A/V (g/m/s)
Low A/V	7436.01	Horjand	30.8	57.34	19	6.1	999	1.85	6.24	3.38	0.30
	5014	Laleh Zar	29.6	56.79	9	5.7	678	0.77	2.17	1.42	0.35
	3749	Chatrood	30.8	56.94	20	5	852	0.15	0.36	0.21	0.40
	4027.02	Chalan Choolan	33.6	48.97	8	5.3	428	1.53	3.40	1.26	0.45
	5006	Torbate Heiydaryeh	35.3	59.26	4	5.9	306	4.38	7.63	2.29	0.57
	1492.06	Zarrat	29	52.74	16	5.6	800	2.22	3.50	0.66	0.64
	3239.01	Abad	29	51.32	6	5.4	482	3.72	5.16	1.12	0.72
Middle A/V	6063.01	Dalaki	29.4	51.36	11	5.7	971	2.00	2.35	0.87	0.85
	5801.07	Shonbeh	28.5	51.66	12	5.1	1396	2.03	2.10	0.76	0.97
	6485	Rivash	35.4	58.48	9	5.5	428	1.90	1.77	0.39	1.07
	8555	Pak Dasht1	38.4	46.66	14	4.5	504	0.09	0.09	0.04	1.09
	2523.01	Ghaemiyeh	29.9	51.69	13	5	617	0.40	0.37	0.08	1.09
	4704	Tazeh-Shahr	35.8	50.9	8	4.9	301	0.25	0.23	0.06	1.09
	5449	Murmuri	32.9	47.72	17	5.5	898	1.55	1.35	0.39	1.15
High A/V	3365.03	Hasan Keyf	36.4	51.29	19	5.3	339	0.44	0.37	0.05	1.20
	5371	Do Ab	27.8	53.51	10	4.6	409	0.19	0.15	0.04	1.25
	8162.02	Qasr-e-Shirin1	29	52.63	6	4.6	347	0.84	0.63	0.15	1.33
	5928.04	Goharan	26.7	57.83	18	5.7	756	1.34	0.96	0.26	1.40
	5016.02	Eshkanan	27.1	53.65	13	5.1	1066	2.64	1.73	0.43	1.52
	5893.03	Shonbeh	28.5	51.78	11	5	1396	1.59	0.95	1.04	1.67
	5801.79	Shonbeh	34.3	45.69	18	6.3	1396	0.37	0.21	0.09	1.78

Table 2
Characteristics of some of the far-field records used in this study.

A/V Range	Record ID	Station Name	Lat.	Long.	R_{rup} (km)	Mw	$V_{S(30)}$ (m/s)	PGA (g)	PGV (m/sec)	PGD (m)	A/V (g/m/s)
Low A/V	7332	Dasht-e-Abbas	34.8	45.9	320	7.3	342	0.19	2.31	3.02	0.08
	5849	Reygan	28.2	62.1	309	7.8	437	0.07	0.68	1.22	0.10
	1758	Torbate Heiydaryeh	33.8	59.8	170	6.9	306	0.38	1.02	1.20	0.37
	1497	Farrashband	29	52.6	54	5.8	630	0.14	0.30	0.20	0.48
	1752.02	Rivash	33.8	59.8	222	6.9	428	0.14	0.24	0.09	0.57
	6998	Chakhmagh	35.9	60.4	84	6.1	1196	0.26	0.38	0.18	0.69
	3466.01	Kelvans	38.9	44.9	28	5.3	549	0.26	0.33	0.12	0.79
Middle A/V	5814.05	Faryab	28.4	51.8	66	5.7	827	0.45	0.55	0.18	0.81
	3545	Gorgan1	37.2	54.4	37	6.2	291	1.08	1.31	0.36	0.82
	2787.03	Bak Kandi	35.7	48.9	101	6.4	308	0.41	0.43	0.43	0.96
	5060	Davaran	29.6	56.8	124	5.7	752	0.12	0.12	0.08	0.98
	1816.04	Afin	34	59.5	57	5.7	1397	0.30	0.27	0.21	1.09
	3236	Delvar	29	51.3	37	5.4	336	0.61	0.55	0.16	1.11
	1934	Damirchi	38.8	48.6	133	5.9	1241	0.43	0.37	0.11	1.14
High A/V	7008	Mashhad1	35.9	60.4	86	6.1	748	0.44	0.36	0.14	1.22
	5693	Kowli	34.5	60	76	5.2	503	0.15	0.12	0.04	1.24
	6671.02	Masjed Soleyman	32.1	49.7	39	5.1	708	0.94	0.67	0.10	1.40
	3237	Saed Abad	29	51.3	46	5.4	921	0.50	0.34	0.19	1.48
	4035.06	Tooshk-e-Ab-e-Sard	33.8	48.8	21	5	891	0.53	0.32	0.04	1.64
	4994.01	Eshkanan	27.2	53.9	32	5.9	1066	2.87	1.59	0.60	1.81
	5125.02	Lamerd	27.1	53.7	53	5.1	881	0.80	0.42	0.12	1.94

Fig. 7. Peak ground acceleration versus peak ground velocity for the three low, middle, and high A/V record groups.

According to Fig. 7, the number of records in each A/V range defined is shown in Table 3. Of the 1744 records examined for far-field earthquakes, 1422, 237, and 85 records belonged to the low, middle, and high A/V categories, respectively. Also, among the 309 records studied for near-field earthquakes, 211, 71, and 27 belonged to the low, middle, and high A/V categories, respectively.

Table 3
Number of records in each A/V category.

A/V Range	Far-field earthquakes	Near-field earthquakes
Low A/V	1422	211
Middle A/V	237	71
High A/V	85	27
Sum	1744	309

The minimum and maximum values of each A/V range in the considered far- and near-field earthquakes are shown in Table 4. As can be seen, the maximum value in the high A/V range of the near-field earthquakes was greater than that corresponding to the far-field earthquakes, and the ranges of A/V in the near- and far-field earthquakes considered were generally close to each other.

Table 4
The minimum and maximum values of each A/V range of the considered far- and near-field earthquakes.

	Far-field earthquakes			Near-field earthquakes		
	Low A/V	Middle A/V	High A/V	Low A/V	Middle A/V	High A/V
Min	0.08	0.80	1.21	0.12	0.80	1.22
Max	0.80	1.20	2.22	0.79	1.20	2.50

3. Ground motion intensity measures

The ground motion intensity measures (IMs) have been characterized by numerous seismic parameters. This study used Matlab codes to calculate the mean period (T_m). Also, the Seismo Signal 2020 software, developed by Seismo Soft [45], was utilized for obtaining other ground motion IMs. The obtained A/V and IM values were entered in Microsoft Excel to plot the diagrams needed. The power regression diagrams for the far- and near-field earthquakes were drawn to indicate the relationship between IMs and A/V. The linear correlation coefficient (r) was calculated to measure the direction and strength of the relationship with the considered IMs. Therefore, the determination coefficient (R^2) was computed for measuring the changes in A/V described by the IMs. The correlation between A/V and the considered IMs are presented in the following sections:

3.1. PGA, PGV, and PGD

One of the crucial parameters in seismic design codes is the peak ground acceleration (PGA) parameter, used to plot seismic hazard maps. This parameter shows the maximum ground acceleration that occurs during an earthquake in a location. The integration of the acceleration time histories gives the peak ground velocity (PGV) parameter. The double integration of the

acceleration time histories gives the peak ground displacement (PGD) parameter. PGA is considered a fine measurement parameter for determining the damage to structures during intermediate earthquakes. Conversely, PGD is regarded as the weakest measurement parameter for this purpose. Also, PGV prepares the best relation to loss in strong earthquakes [46–48].

A summary of the results is given in Tables 1 and 2, which indicate that the average PGA values in the near- and far-field earthquakes considered were equal to 0.73g and 0.35g, respectively. Also, the mean PGV values for the near- and far-field earthquakes considered were 1.19 and 0.75 m/s, respectively. Furthermore, the mean PGD values for the near- and far-field earthquakes were 0.53 and 0.43 m, respectively. As mentioned before, the results show that the mean value of the far-field records was lower than that of the near-field records.

3.2. Average spectral acceleration

($S_{a,avg}$) is the spectral acceleration of geometric average of a certain number of periods with a five percent damping geometric average. The $S_{a,avg}$, compared to the traditional IMs, is a useful and practicable measure of structural response [49]. As well, the study by Kohrangi et al. showed that $S_{a,avg}$ could present a fine prediction of the local and global linear responses in the vicinity of buildings [50].

Figure 8 shows the A/V data plotted against $S_{a,avg}$. It also includes the analysis of power regression for the far and near-field strong ground motion. The near- and far-field record's residual standard deviation (σ) were respectively equal to 0.124 and 0.103. Furthermore, the negative coefficient of correlation (R^2) value in the near-field earthquakes was equal to 0.0049 (r = 0.07), i.e., 0.5% of the total changes in A/V could be investigated by the power regression of $S_{a,avg}$ and A/V. Also, the negative coefficient of correlation (R^2) value in the far-field earthquakes was equal to 0.0079 (r = 0.089), i.e., 0.7% of the total changes in A/V could be investigated by the power regression of $S_{a,avg}$ and A/V. Thus, it can be said that there is a very weak correlation between $S_{a,avg}$ and A/V in the near- and far-field records.
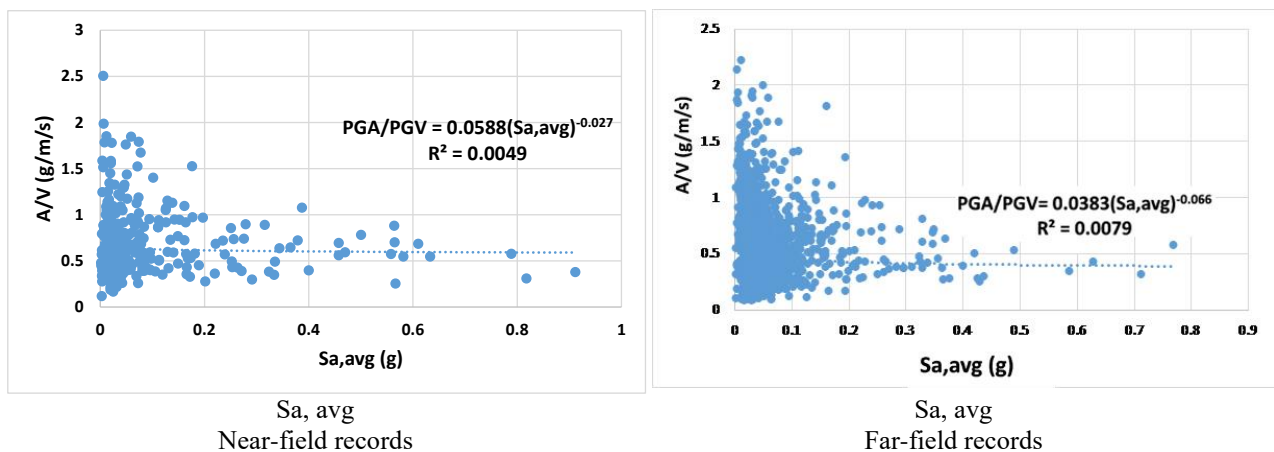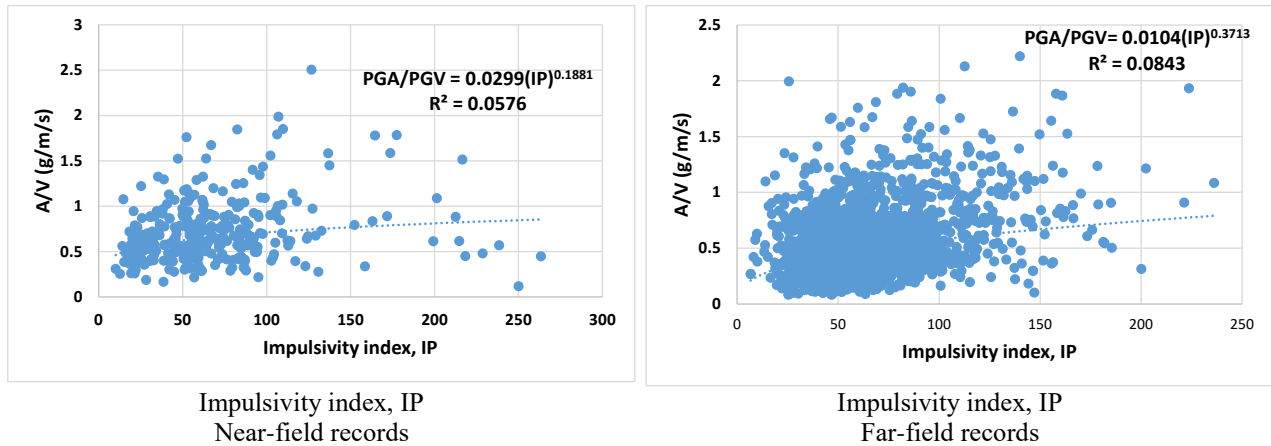

Near-field records   Far-field records
Fig. 8. Graphs of A/V versus $S_{a,avg}$ for near- and far-field records.

3.3. Impulsivity index

Many studies have shown that the severe-velocity pulse motions adversely affect structures' seismic performance [51,52]. The impulsivity index (IP), used for identifying the pulse-like ground motions, is calculated by the following equation [53]:

$$IP = \frac{Ld_v}{PGV} \tag{1}$$

where Ld_v denotes the length reached by the trace of velocity records, and PGV denotes the peak ground velocity.

Impulsivity index, IP
Near-field records

Impulsivity index, IP
Far-field records

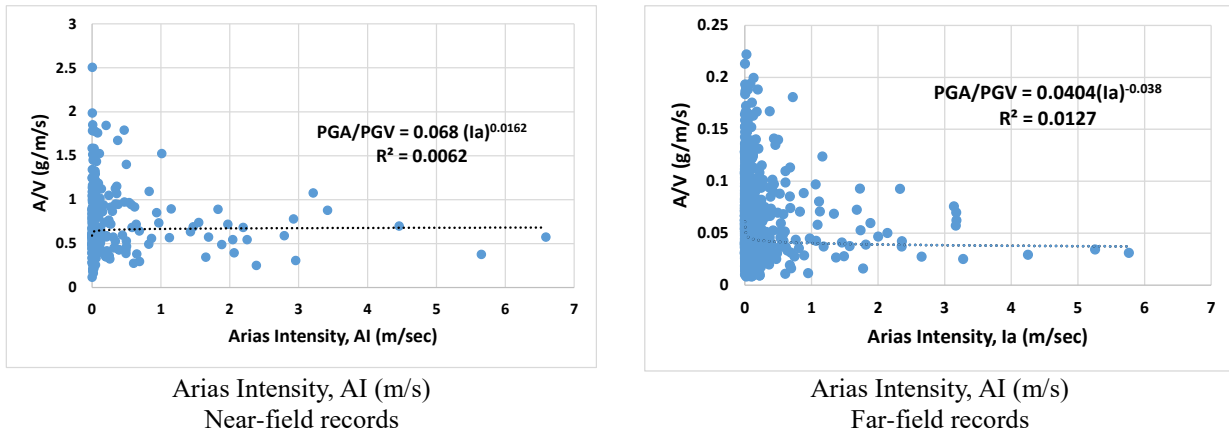**Fig. 9.** Graphs of A/V versus IP for near- and far-field records.

Figure 9 shows the A/V data plotted against IP. It also includes the analysis of power regression for the far and near-field strong ground motion. The near- and far-field record's residual standard deviation (σ) were respectively equal to 0.119 and 0.092. Furthermore, the positive coefficient of correlation (R^2) value in the near-field earthquakes was equal to 0.0576 (r = 0.24), i.e., 5.7% of the total changes in A/V could be investigated by the power regression of IP and A/V. Also, the positive coefficient of correlation (R^2) value in the far-field earthquakes was equal to 0.0843 (r = 0.29), i.e., 8.4% of total changes in A/V could be investigated by the power regression of IP and A/V. Such results reveal that IP and A/V have a weak correlation in both the near- and far-field records.

3.4. Arias intensity

Arias intensity (AI) is an acceptable response parameter for identifying damage to structures, particularly those with short periods [54]. AI is defined as the integral of all squared ground acceleration values with respect to time[55] as in the following:

$$AI = \frac{\pi}{2g} \int_0^{T_d} a(t)^2 dt \ (m/s) \tag{2}$$

where T_d is the total ground motion time, g is gravitational acceleration, and a(t) refers to the recorded acceleration time history values.

Arias Intensity, AI (m/s)
Near-field records

Arias Intensity, AI (m/s)
Far-field records

Fig. 10. Graphs of A/V versus AI for near- and far-field records.

Figure 10 illustrates A/V data plotted against AI. It also includes the analysis of power regression for the far and near-field strong ground motion. The near- and far-field record's residual standard deviation (σ) were respectively equal to 0.126 and 0.103. Furthermore, the positive coefficient of correlation (R^2) value in the near-field earthquakes was equal to 0.0062 (r = 0.249), i.e., 0.62% of the total changes in A/V could be investigated by the power regression of AI and A/V. As well, the negative coefficient of correlation (R^2) value in the far-field earthquakes was equal to 0.0127 (r = 0.113), i.e., 1.3% of total changes in A/V could be investigated by the power regression of AI and A/V. Such results reveal that AI and A/V have a weak correlation in both the near- and far-field records.

3.5. Predominant period

Predominant period (Tp) is the period during which the maximum spectral acceleration occurs in an acceleration response spectrum calculated at five percent damping. Figure 11 shows A/V data plotted against Tp. It also includes the analysis of power regression for the far and near-field strong ground motion. The near- and far-field record's residual standard deviation (σ) were respectively equal to 0.134 and 0.122. Furthermore, the negative coefficient of correlation (R^2) value in the near-field earthquakes was equal to 0.2189 (r = 0.468), i.e., 22% of the total changes in A/V could be investigated power regression of T_p and A/V. As well, the negative coefficient of correlation (R^2) value in the far-field earthquakes was equal to 0.2349 (r = 0.485), i.e., 23% of the total changes in A/V could be investigated by the power regression of T_p and A/V. Such results reveal that these parameters have a moderate correlation in both the near- and far-field earthquakes.

Predominant period, Tp (s)
Near-field records

Predominant period, Tp (s)
Far-field records
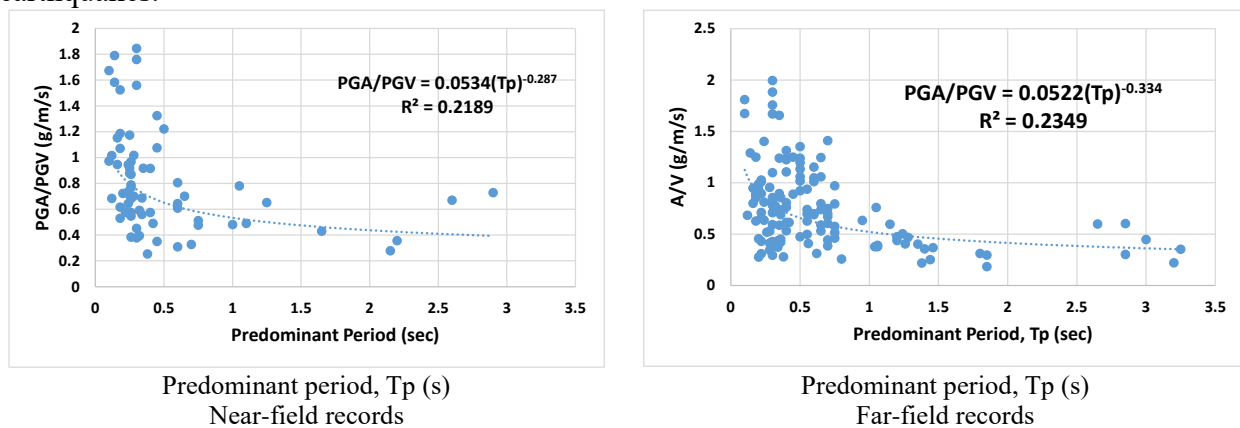
Fig. 11. Graphs of A/V versus Tp (s) for near- and far-field records.

3.6. A95 parameter

Because PGA is often associated with high-frequency ground motions which do not possess high energy, the A95 parameter has been proposed as an alternative IM. A95 is an acceleration level that contains up to 95% of the Arias intensity. Based on this description, PGA is considered equal to A100, and a 95% level is selected so that it is as close to the peak as possible. A95 is obtained as follows [56]

$$E_x/E_s = \exp(-3.13(A/A_{95})^{1.48}$$
$$A_{95} = 0.764E_s^{0.438}$$
$$logE_s = -4.05 + 0.77M - 0.85logR - 0.0081R, R > 30km$$
$$logE_s = -18.52 - 1.67M + 11.58M^{1/2} - 0.32logR - 0.007R, R < 30km$$

(3)

where E_x is a fraction of the Arias intensity above an acceleration level A, E_s is the Arias intensity, M is the surface wave magnitude, and R is the shortest distance to the energy source, known as the focal distance in km.

A95 (g)
Near-field records

A95 (g)
Far-field records
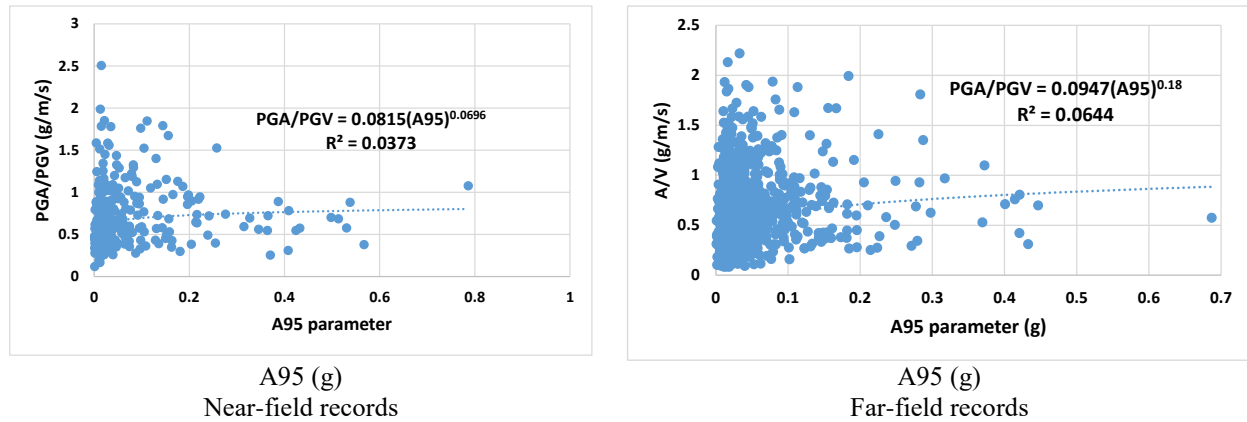
Fig. 12. Graphs of A/V versus A95 for near- and far-field records.

In Figure 12, A/V data are plotted against A95. This figure also includes the analysis of power regression for the far and near-field strong ground motion. The near- and far-field record's residual standard deviation (σ) were respectively equal to 0.126 and 0.01 for the near and far-field earthquake records. Furthermore, the positive coefficient of correlation (R^2) value in the near and far-field records were respectively equal to 0.0373 (r = 0.193), i.e., 3.78% of the total changes in A/V could be investigated by power regression of A95 and A/V. As well, the positive coefficient of correlation (R^2) value in the far-field earthquakes was equal to 0.0644 (r = 0.254), i.e., 6.4% of total changes in A/V could be investigated by power regression of A95 and A/V. Such results reveal that these parameters also have a weak correlation in both the near- and far-field records.

3.7. Mean period

Rathje et al., whose work focused on three frequency contents parameters, found the mean period (Tm) to be the best simplified frequency content characterization parameter. They

developed an empirical model that describes the mean period's distance, magnitude, and site. The mean period can be calculated using the following equation [27]:

$$T_m = \frac{\sum c_i^2 / f_i}{\sum c_i^2} \tag{4}$$

where f_i denotes the discrete Fourier transform of frequencies ranging from 0.25 to 20 Hz, and C_i denotes the Fourier amplitudes.

Mean Period, T_m (s)
Near-field records

Mean period, T_m (s)
Far-field records
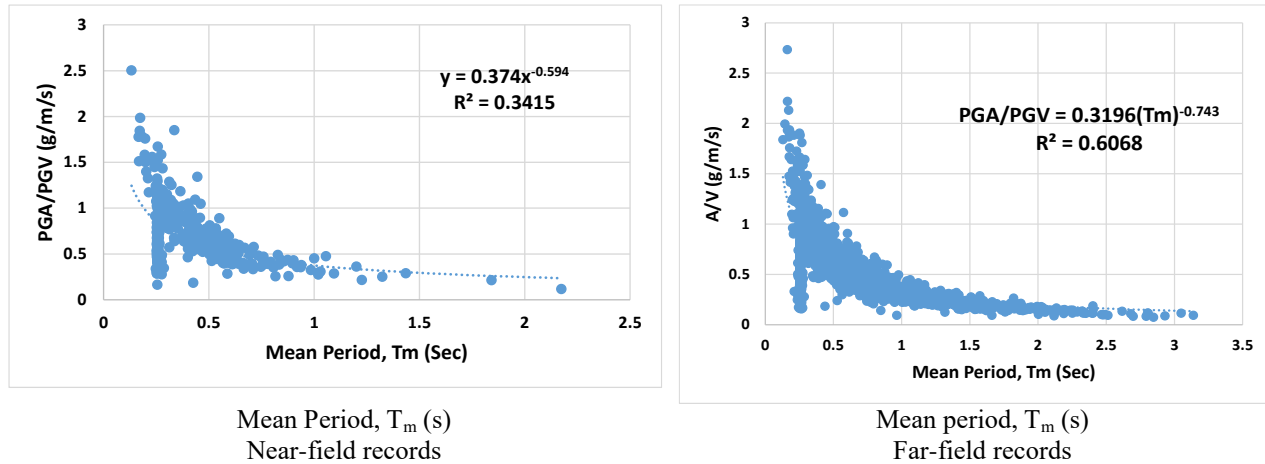
Fig. 13. Graphs of A/V versus T_m for the near- and far-field records.

Figure 13 shows A/V data plotted against T_m. It also includes the analysis of power regression for the far and near-field strong ground motion. The near- and far-field record's residual standard deviation (σ) were respectively equal to 0.094 and 0.062. Furthermore, the negative coefficient of correlation (R^2) value in the near-field earthquakes was equal to 0.3415 (r = 0.584), i.e., 34% of the total changes in A/V could be investigated by the power regression of T_m and A/V. As well, the negative coefficient of correlation (R^2) value in the far-field earthquakes was equal to 0.6068 (r = 0.779), i.e., 61% of the total changes in A/V could be investigated by the power regression of T_m and A/V. These results indicate that the relationship between T_m and A/V in the far-field records is stronger than that in the near-field earthquakes.

3.8. Cumulative absolute velocity

The cumulative absolute velocity (CAV) is the integral of the absolute acceleration time series rather than the squared acceleration time series used in calculating AI [57]:

$$CAV = \int_0^{T_d} a(t) dt \tag{5}$$

where T_d is the total recorded ground motion time and, $a(t)$ is the absolute acceleration value at time t. CAV has widespread use in engineering practices and could be considered as a measure of damage to structures [58].

Figure 14 illustrates A/V values plotted against CAV. It also includes the analysis of power regression for the far and near-field strong ground motion. The near- and far-field record's residual standard deviation (σ) were respectively equal to 0.125 and 0.099. Furthermore, the negative coefficient of correlation (R^2) value in the near-field earthquakes was equal to 0.0032 (r

= 0.057), i.e., 0.32% of total changes in A/V could be investigated by the power regression of CAV and A/V. As well, the negative coefficient of correlation (R^2) value in the far-field earthquakes was equal to 0.1059 (r = 0.325), i.e., 11% of total changes in A/V could be investigated by the power regression of CAV and A/V. Such results reveal that these parameters also have a very weak correlation in the near-field earthquakes and a weak correlation in the far-field earthquakes. Therefore, it could be concluded that the correlation in the far-field records is stronger than that in the near-field records.


CAV (m/s)
Near-field records

CAV (m/s)
Far-field records
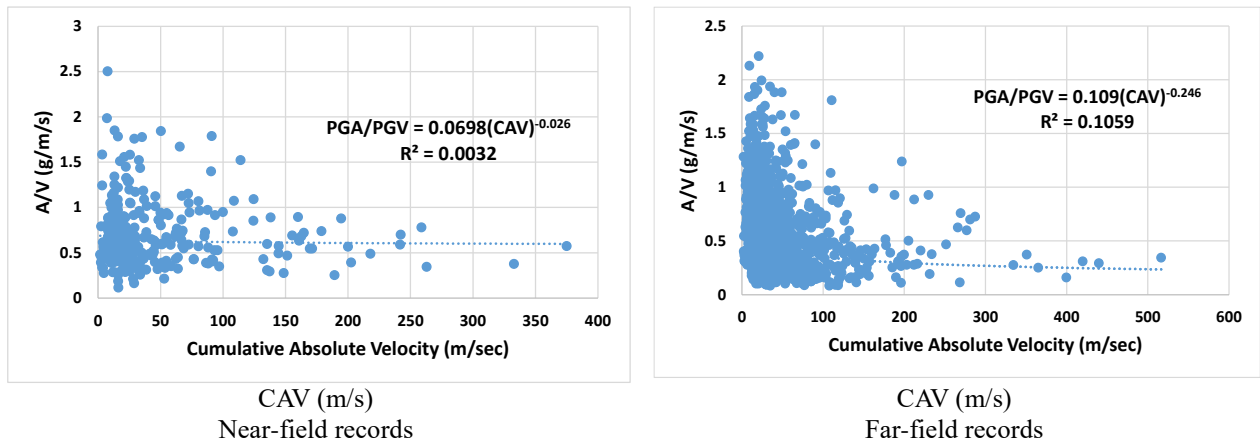
Fig. 14. A/V versus CAV for near- and far-field records.

3.9. Number of effective cycles

The number of effective cycles (N_{cy}) parameter, proposed by Malhotra in 2002, is calculated by the following equation [59]:

$$N_{cy} = \frac{1}{2}\sum_{i=1}^{2n}(\frac{u_i}{u_{max}})^2 \qquad (6)$$

where u_{max} denotes the amplitude of the largest half cycle, u_i denotes the amplitude of ith half cycle, and n is the total number of half cycles. The number of motion cycles is of great importance in earthquake engineering. This number is a significant factor in seismic design and assessing damage to structures, although no consensus has been reached on this subject [60].

Number of effective cycles, Ncy
Near-field records

Number of effective cycles, Ncy
Far-field records
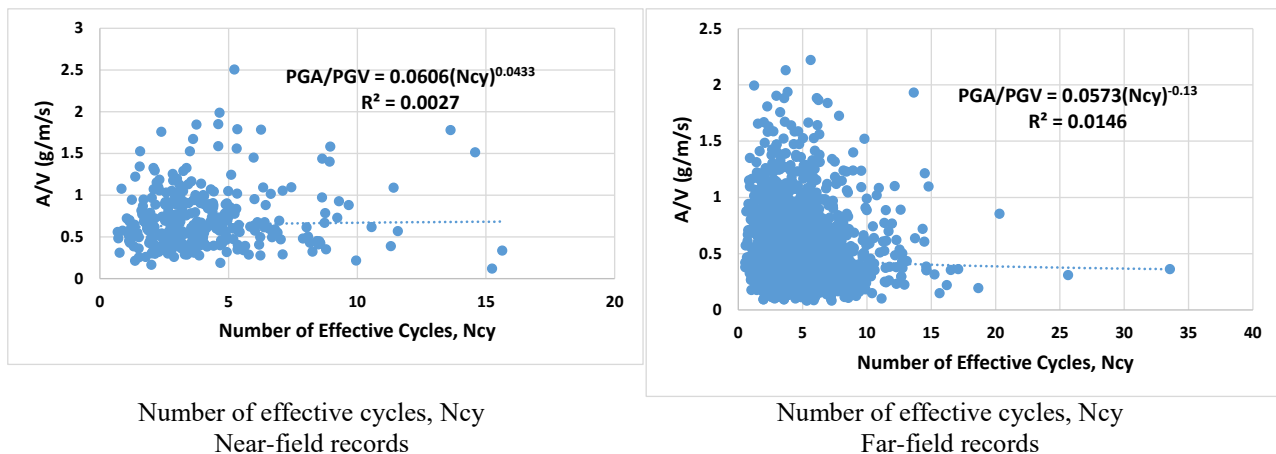
Fig. 15. Graphs of A/V versus Ncy for the near- and far-field records.

Figure 15 shows A/V data plotted against N_{cy}. It also includes the analysis of power regression for the far and near-field strong ground motion. The near- and far-field record's residual standard deviation (σ) were respectively equal to 0.125 and 0.102. Furthermore, the positive coefficient of correlation (R^2) value in the near-field earthquakes was equal to 0.0027 (r = 0.052), i.e., 0.27% of total changes in A/V could be investigated by the power regression of N_{cy} and A/V. As well, the negative coefficient of correlation (R^2) value in the far-field earthquakes was equal to 0.0146 (r = 0.121), i.e., 1.5% of the total changes in A/V could be investigated by the power regression of N_{cy} and A/V. Such results reveal that these parameters have a very weak correlation in both the near-field and far-field records.

3.10. Damage index

Damage index (DI) is the summation of the amplitudes of cycles in accelerograms, raised to the power of c and multiplied by the linear scale factor C. The corresponding equation is as follows [59]:

$$DI = C \cdot \sum_{i=1}^{n} u_i^c \tag{7}$$

where n is the number of half-cycles and u_i is the deformation amplitude of the ith half-cycle.

Figure 16 shows A/V data plotted against DI. It also includes the analysis of power regression for the far and near-field strong ground motion. The near- and far-field record's residual standard deviation (σ) were respectively equal to 0.125 and 0.102. Furthermore, the positive coefficient of correlation (R^2) value in the near-field earthquakes was equal to 0.061 (r = 0.247), i.e., 6.1% of the total changes in A/V could be investigated by the power regression of DI and A/V. As well, the negative coefficient of correlation (R^2) value in the far-field earthquakes was equal to 0.0762 (r = 0.276), i.e., 7.6% of the total changes in A/V could be investigated by the power regression of DI and A/V. Such results reveal a weak correlation among these parameters in both the near-field and far-field records.
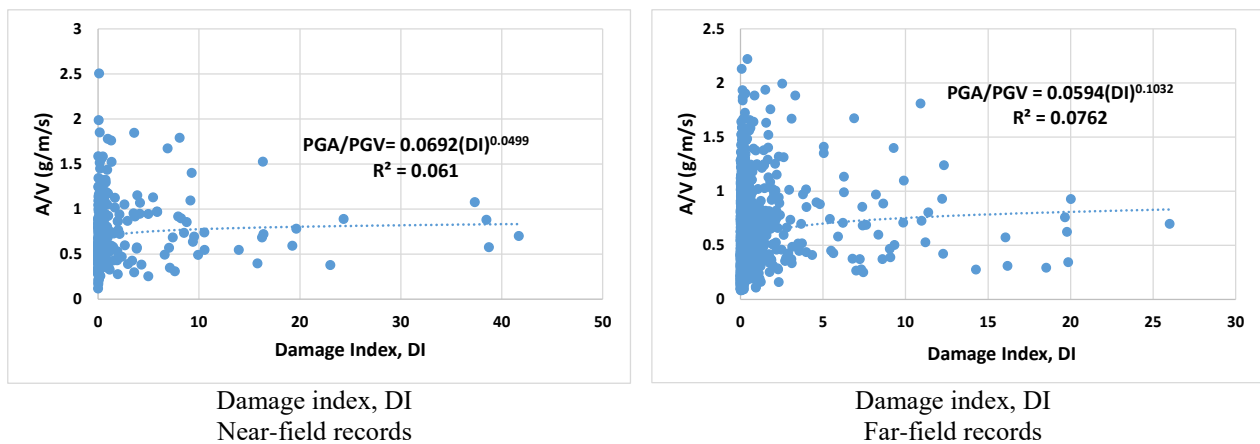

Damage index, DI
Near-field records   Far-field records
Fig. 16. Graphs of A/V versus DI for near- and far-field records.

3.11. Housner intensity

Housner intensity (HI) is calculated using the equation below [61]:

$$HI = \int_{0.1}^{2.5} PSV(\varepsilon = 0.05, t)dt \tag{8}$$
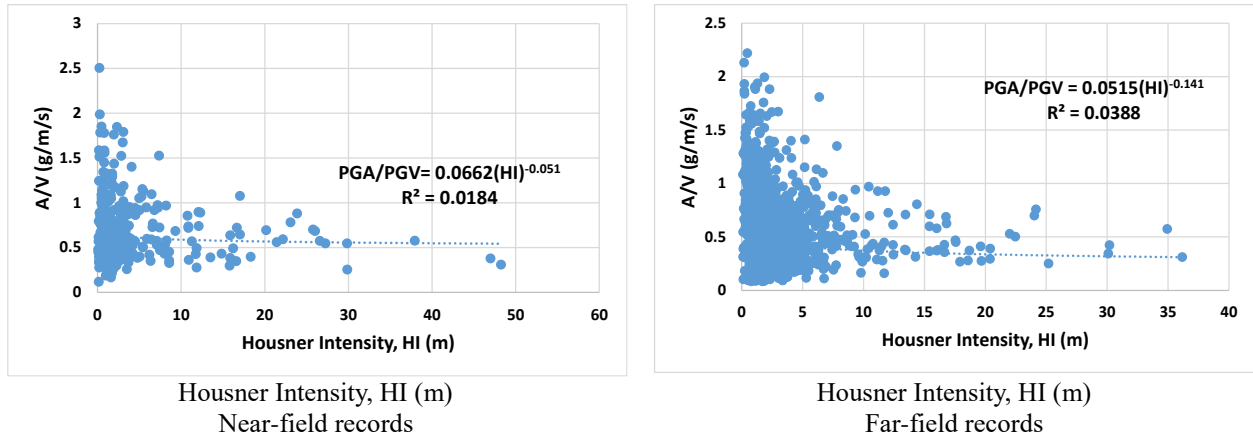
where PSV is the pseudo-velocity response spectrum.

Fig. 17. A/V versus HI for near- and far-field records.

Figure 17 shows A/V data plotted against HI. It also includes the analysis of power regression for the far and near-field strong ground motion. The near- and far-field record's residual standard deviation (σ) were respectively equal to 0.123 and 0.102. Furthermore, the negative coefficient of correlation (R^2) value in the near-field earthquakes was equal to 0.0184 (r = 0.136), i.e., 1.8% of total changes in A/V could be investigated by the power regression of HI and A/V. As well, the negative coefficient of correlation (R^2) value in the far-field earthquakes was equal to 0.0388 (r = 0.197), i.e., 3.9% of total changes in A/V could be investigated by the power regression of HI and A/V. Such results reveal that these parameters have a very weak correlation in both the near- and far-field records.

4. Discussion

Table 5 presents the calculated coefficients of correlation among A/V and the considered IMs for the near-field and far-field earthquakes. The correlations were investigated in the form of power regression of the IMs and the different A/V values of the low, middle, and high ranges defined based on Tso et al.'s 1992 and Naumoski et al.'s 1988 works [8,34]. According to this table, for the near- and far-field records, Tm had the highest rank among the other IMs. Moreover, in the near-field earthquakes with high A/V, it had the maximum correlation, and in the far-field earthquakes with a low A/V, it had the minimum correlation. The correlation of Tm was stronger for the far-field earthquakes than for the near-field earthquakes. Tp also ranked among the IMs with the highest correlation in the near- and far-field records. It had the maximum correlation in the near-field earthquakes with a high A/V and the far-field earthquakes with a middle A/V. Ncy was recognized to have the lowest correlation among IMs parameters in the near-field earthquakes so that for a low A/V, it had the minimum R^2 value. $S_{a,avg}$ was also found to have the lowest correlation among IMs parameters so that for a low A/V, it had the minimum R^2 value. It should be noted that all these conclusions are specific to the Iran region data that has been examined in this study.

Table 5
R^2 between A/V and the considered IMs for the near- and far-field records.

IMs	Far-field earthquakes				Near-field earthquakes			
	Low A/V	Middle A/V	High A/V	ALL A/V	Low A/V	Middle A/V	High A/V	ALL A/V
AI	0.0172	0.001	0.0055	0.0127	0.0037	0.0101	0.00006	0.0062
CAV	0.0982	0.0028	0.0021	0.1059	0.0016	0.0087	0.000006	0.0032
HI	0.0024	0.0361	0.0079	0.0388	0.00001	0.0027	0.0533	0.0184
A95	0.0396	0.0002	0.0184	0.0644	0.0078	0.0197	0.0074	0.0373
Tp	0.1342	0.1806	0.1567	0.2349	0.0651	0.1691	0.3249	0.2189
Tm	0.5054	0.1571	0.3646	0.6068	0.1364	0.1674	0.3947	0.3415
Ncy	0.0163	0.0023	0.0002	0.0146	0.003	0.0019	0.1134	0.0027
DI	0.0507	0.0006	0.0226	0.0762	0.0389	0.0187	0.0064	0.061
Ip	0.0459	0.029	0.0148	0.0843	0.0036	0.0008	0.2231	0.0576
Sa,avg	0.0027	0.0343	0.0064	0.0079	0.0034	0.0042	0.0433	0.0049

5. Artificial neural network model

In the previous sections, regression models were employed to relate A/V parameter to other intensity measures. It is then explored that which of intensity measures provides the best predictability for A/V parameter. The dependence of results on the utilized mathematical model is investigated in this section. In this section, an Artificial Neural Network model, as an alternative mathematical tool, is adopted to predict A/V parameter as a function of other intensity measure parameters. It is investigated that whether Artificial Neural Network (ANN) offers better predictions than regression models or not. ANN is a mathematical and computational tool inspired from networks of biological neurons. In this section, an ANN model is developed for predicting A/V from mean period (T_m) for far-field ground motions. The accuracy of this ANN model is then compared with the counterpart of regression model. Three layers feedforward neural network is used here. The structure of this model is shown in Figure 18. As can be seen, input layer and output layer have one node because this model takes one variable (T_m) as input and return one variable (A/V) as output. Six nodes are used in hidden layer. Sigmoid is employed for activation function. The utilized activation function is depicted in Figure 19. This activation function is implemented by "tansig" in MATLAB.

Input Neurons   Hidden Neurons   Output Neurons
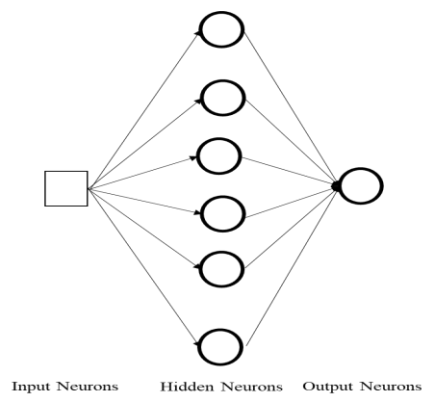
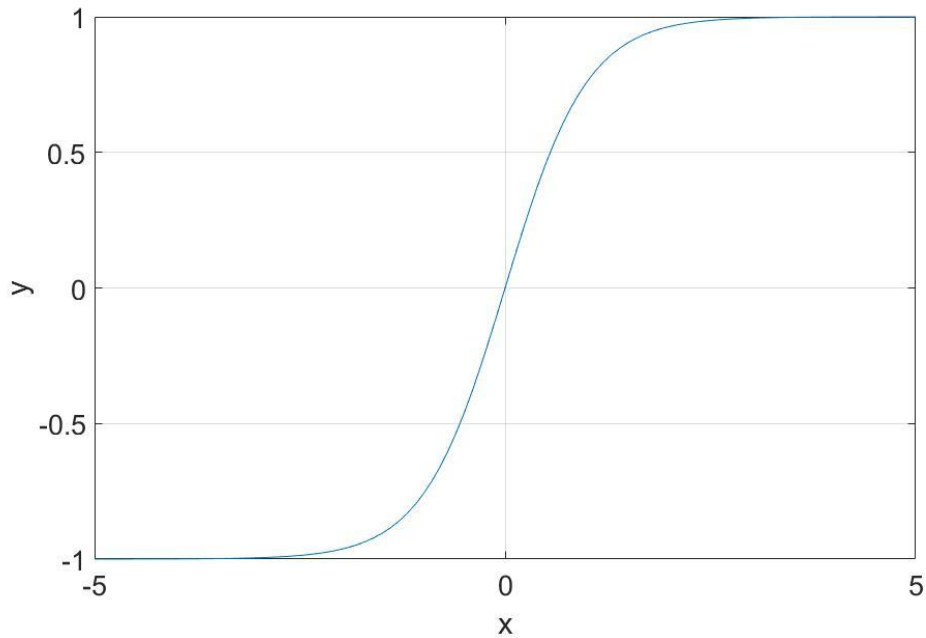**Fig. 18.** Utilized 3-layer feedforward neural network.

Fig. 19. Utilized activation function (tansig).

All data is randomly divided into three groups of training data, validation data, and test data by the proportion of 70%, 15%, and 15%, respectively. The training process of the network is illustrated in Figure 20.
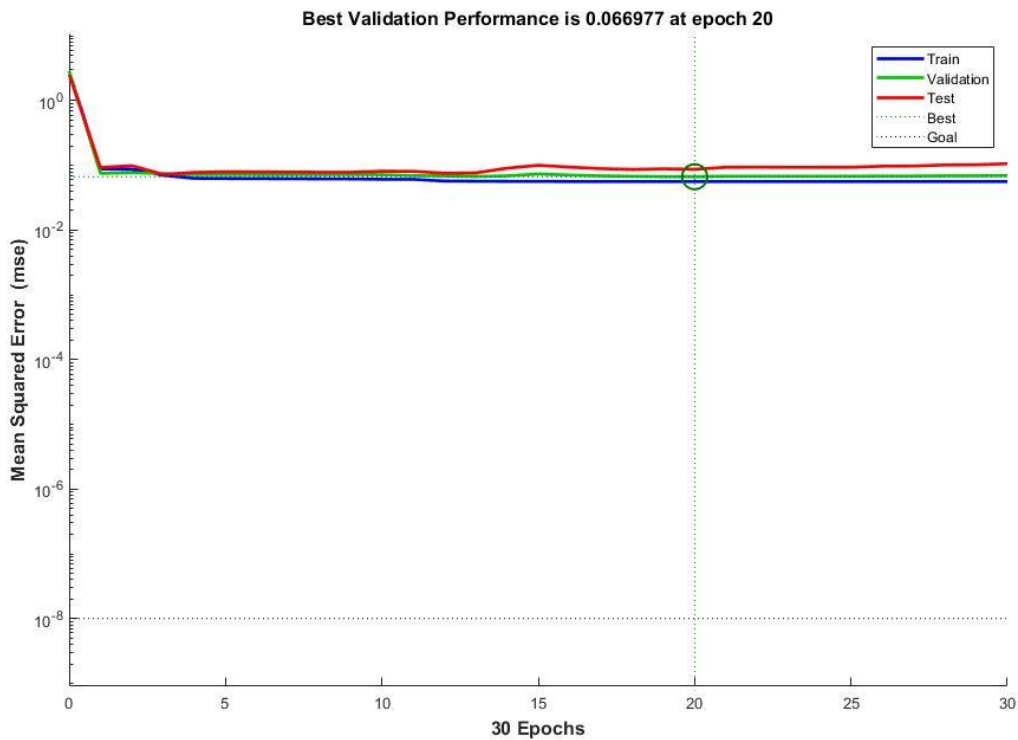

Fig. 20. Training process of the Artificial Neural Network.

In order to quantify the accuracy of the developed ANN model and compare it with regression model results, root mean square error (RMSE) is used, as defined below.

$$RMSE = \sqrt{\frac{1}{N} \sum_1^N e_i^2}$$ (9)

Where e_i is the prediction error associated with i-th data point and N is the total amount of data. RMSE of the ANN model is 0.2501 and RMSE of the regression model is 0.2901. This finding shows that using the ANN model is preferred for predicting A/V as compared to regression models. The improvement of accuracy by using the ANN model is about 15%.

6. Conclusion

This research investigated the relationship between the intensity measure parameters (IMs) and peak ground acceleration to peak ground velocity ratio (A/V) for the Iran region data records provided by the Iran Strong Motion Network (ISMN) of the Building and Housing Research Center (BHRC). The database included 2053 strong ground motion records until 2021 with the moment magnitude from 4.5 to 7.8, rupture distance from 1 to 600 km, and average shear wave velocity from 155 to 1594 m/s. The records were divided into two categories of near-field earthquakes with rupture distances of less than 20 km and far-field earthquakes with rupture distances of more than 20 km. The A/V values of the record were obtained and categorized into three ranges; 0.8 g/m/s > PGA/PGV for the low range A/V, PGA/PGV > 1.2 g/m/s for the high range A/V and $0.8\,g/m/s \leq PGA/PGV \leq 1.2\,g/m/s$ for the middle A/V. The IMs that were investigated included peak ground acceleration (PGA), peak ground velocity (PGV), peak ground displacement (PGD), A/V, average spectral acceleration ($S_{a,avg}$), impulsivity index (IP), Arias intensity (AI), predominant period (T_p), A95 parameter, mean period (Tm), cumulative absolute velocity (CAV), number of effective cycles (N_{cy}), damage index (DI), and Housner intensity (HI) corresponding to the near- and far-field ground motions. The A/V data was plotted against these IMs, and regression analysis was performed. It should be mentioned that the results of this study are limited to the studied data and the type of regression analysis. No significant difference was observed between the A/V values of the near- and far-field records considered in this study. In both the near- and far-field earthquakes, A/V was found to have a negligible correlation with $S_{a,avg}$, AI, CAV, N_{cy}, and HI parameters. On the other hand, A/V was observed to have a stronger correlation with the mean period (T_m) parameter, compared to the other IMs investigated in this study. Finally, an Artificial Neural Network model is developed to predict A/V parameter as a function of T_m. Results show that ANN can effectively be used to predict A/V and provides 15% more accuracy as compared to regression models.

Acknowledgments

List of abbreviations

The following symbols are used in this paper

Abbreviations	Explanation
AI	Arias Intensity
BHRC	Building and Housing Research Center
CAV	Cumulative Absolute Velocity
DI	Damage Index
HI	Housner Intensity
IMs	Intensity Measures
ISMN	Iran Strong Motion Network
IP	Impulsivity index
Mw	Moment Magnitude
N_{cy}	Number of effective cycles
PGA	Peak Ground Acceleration
PGV	Peak Ground Velocity
PGD	Peak Ground Displacement
A/V	Peak Ground Acceleration/Peak Ground Velocity ratio
R_{rup}	Rupture distance
$S_{a,avg}$	Average Spectral Acceleration
T_m	Mean Period
Tp	Predominant Period
V_{s30}	Shear velocity in the top 30m

References

[1]   Hassanzadeh R. Earthquake population loss estimation using spatial modelling and survey data: The Bam earthquake, 2003, Iran. Soil Dyn Earthq Eng 2019;116:421–35. https://doi.org/10.1016/j.soildyn.2018.09.023.

[2]   Xu R, Fatahi B. Novel application of geosynthetics to reduce residual drifts of mid-rise buildings after earthquakes. Soil Dyn Earthq Eng 2019;116:331–44. https://doi.org/10.1016/j.soildyn.2018.10.022.

[3]   Ghaedi Vanani AA, Shoaei G, Zare M. Statistical analyses of landslide size and spatial distribution triggered by 1990 Rudbar-Manjil (Mw 7.3) earthquake, northern Iran: revised inventory, and controlling factors. Bull Eng Geol Environ 2021;80:3381–403. https://doi.org/10.1007/s10064-021-02106-8.

[4]   Harati M, Mashayekhi M, Estekanchi HE. Correlation of Ground Motion Duration with Its Intensity Metrics: A Simulation Based Approach. J Soft Comput Civ Eng 2020;4:17–39. https://doi.org/10.22115/scce.2020.227576.1207.

[5]   Du W. Empirical Correlations of Frequency-Content Parameters of Ground Motions with Other Intensity Measures. J Earthq Eng 2019;23:1073–91. https://doi.org/10.1080/13632469.2017.1342303.

[6]   Zhu TJ, Tso WK, Heidebrecht AC. Effect of Peak Ground a/v Ratio on Structural Damage. J Struct Eng 1988;114:1019–37. https://doi.org/10.1061/(ASCE)0733-9445(1988)114:5(1019).

[7]   Garg R, Vemuri JP, Subramaniam KVL. Correlating Peak Ground A/V Ratio with Ground Motion Frequency Content, 2019, p. 69–80. https://doi.org/10.1007/978-981-13-0365-4_6.

[8] Tso WK, Zhu TJ, Heidebrecht AC. Engineering implication of ground motion A/V ratio. Soil Dyn Earthq Eng 1992;11:133–44. https://doi.org/10.1016/0267-7261(92)90027-B.

[9] Rezaee Manesh M, Fattahi S, Saffari H. Investigation of earthquake significant duration on the seismic performance of adjacent steel structures in near-source. J Rehabil Civ Eng 2021;9:84–101. https://doi.org/10.22075/JRCE.2020.20373.1410.

[10] Rezaeimanesh M, Saffari H. Relationships Between Significant, Bracketed and Uniform Durations with Earthquake Indices and Site Conditions Using Iranian Seismic Data. Sharif J Civ Eng 2021;37:95–103.

[11] Ale Saheb Fosoul S, Tajmir Riahi H, Hatami N. A New Ground Motion Record Selection Procedure Based on The Effects of Spectral Shape and Period Elongation. Sci Iran 2019;0–0. https://doi.org/10.24200/sci.2019.51546.2246.

[12] Harati M, Mashayekhi M, Ashoori Barmchi M, Estekanchi H. Influence of Ground Motion Duration on the Structural Response at Multiple Seismic Intensity Levels. Numer Methods Civ Eng 2019;3:10–23. https://doi.org/10.29252/nmce.3.4.10.

[13] Kostinakis K, Fontara I-K, Athanatopoulou AM. Scalar Structure-Specific Ground Motion Intensity Measures for Assessing the Seismic Performance of Structures: A Review. J Earthq Eng 2018;22:630–65. https://doi.org/10.1080/13632469.2016.1264323.

[14] Wei B, Hu Z, He X, Jiang L. Evaluation of optimal ground motion intensity measures and seismic fragility analysis of a multi-pylon cable-stayed bridge with super-high piers in Mountainous Areas. Soil Dyn Earthq Eng 2020;129:105945. https://doi.org/10.1016/j.soildyn.2019.105945.

[15] Elhout EA. The correlation between the ground motion intensity measure parameters of earthquakes. Asian J Civ Eng 2020;21:829–40. https://doi.org/10.1007/s42107-020-00243-1.

[16] Hui S, Tang L, Zhang X, Wang Y, Ling X, Xu B. An investigation of the influence of near-fault ground motion parameters on the pile's response in liquefiable soil. Earthq Eng Eng Vib 2018;17:729–45. https://doi.org/10.1007/s11803-018-0472-7.

[17] Kiani A, Torabi M, Mirhosseini SM. Intensity measures for the seismic response evaluation of buried steel pipelines under near-field pulse-like ground motions. Earthq Eng Eng Vib 2019;18:917–31. https://doi.org/10.1007/s11803-019-0543-4.

[18] Kamgar R, Dadkhah M, Naderpour H. Seismic response evaluation of structures using discrete wavelet transform through linear analysis. Structures 2021;29:863–82. https://doi.org/10.1016/j.istruc.2020.11.012.

[19] Kamgar R, Rahgozar P. Optimum location for the belt truss system for minimum roof displacement of steel buildings subjected to critical excitation. Steel Compos Struct An Int J 2020;37:463–79.

[20] Dadkhah M, Kamgar R, Heidarzadeh H. Reducing the Cost of Calculations for Incremental Dynamic Analysis of Building Structures Using the Discrete Wavelet Transform. J Earthq Eng 2022;26:3317–42. https://doi.org/10.1080/13632469.2020.1798830.

[21] Kamgar R, Tavakoli R, Rahgozar P, Jankowski R. Application of discrete wavelet transform in seismic nonlinear analysis of soil–structure interaction problems. Earthq Spectra 2021;37:1980–2012. https://doi.org/10.1177/8755293020988027.

[22] Dadkhah M, Kamgar R, Heidarzadeh H, Jakubczyk-Gałczyńska A, Jankowski R. Improvement of Performance Level of Steel Moment-Resisting Frames Using Tuned Mass Damper System. Appl Sci 2020;10:3403. https://doi.org/10.3390/app10103403.

[23] Salimi M, Kamgar R, Heidarzadeh H. An evaluation of the advantages of friction TMD over conventional TMD. Innov Infrastruct Solut 2021;6:95. https://doi.org/10.1007/s41062-021-00473-5.

[24] Dadkhah M, Kamgar R, Heidarzadeh H. Improving the nonlinear seismic performance of steel moment-resisting frames with minimizing the ductility damage index. SN Appl Sci 2021;3:86. https://doi.org/10.1007/s42452-021-04141-2.

[25] Zhu TJ, Heidebrecht AC, Tso WK. Effect of peak ground acceleration to velocity ratio on ductility demand of inelastic systems. Earthq Eng Struct Dyn 1988;16:63–79. https://doi.org/10.1002/eqe.4290160106.

[26] Sawada T, Hirao K, Yamamoto H, Tsujihara O. Relation between maximum amplitude ratio (a/v, ad/v2) and spectral parameters of earthquake ground motion. Earthq. Eng. Tenth World Conf., vol. 2, 1992, p. 617.

[27] Rathje EM, Abrahamson NA, Bray JD. Simplified Frequency Content Estimates of Earthquake Ground Motions. J Geotech Geoenvironmental Eng 1998;124:150–9. https://doi.org/10.1061/(ASCE)1090-0241(1998)124:2(150).

[28] Rathje EM, Faraj F, Russell S, Bray JD. Empirical Relationships for Frequency Content Parameters of Earthquake Ground Motions. Earthq Spectra 2004;20:119–44. https://doi.org/10.1193/1.1643356.

[29] Bommer JJ, Hancock J, Alarcón JE. Correlations between duration and number of effective cycles of earthquake ground motion. Soil Dyn Earthq Eng 2006;26:1–13. https://doi.org/10.1016/j.soildyn.2005.10.004.

[30] Tavakoli HR, Gilani H, Abdollahzadeh GR. Comparative evaluation of seismic parameters for near-fault and far-fault earthquakes. 15th World Conf. Earthq. Eng., 2012, p. 24–8.

[31] Mashayekhi M, Estekanchi HE, Vafai H. A method for matching response spectra of endurance time excitations via the Fourier transform. Earthq Eng Eng Vib 2020;19:637–48. https://doi.org/10.1007/s11803-020-0586-6.

[32] Oliveira CS, Gassol G, Goula X, Susagna T. A European digital accelerometric database: statistical analysis of engineering parameters of small to moderate magnitude events. Earthq Eng Eng Vib 2014;13:583–97. https://doi.org/10.1007/s11803-014-0265-6.

[33] Huang C, Galasso C. Ground-motion intensity measure correlations observed in Italian strong-motion records. Earthq Eng Struct Dyn 2019;48:1634–60. https://doi.org/10.1002/eqe.3216.

[34] Naumoski N, Tso WK, Heidebrecht AC. A selection of representative strong ground motion earthquake records having different A/V ratios. Report No. EERG 88/01, Earthquake Engineering Research Group, McMaster University, Hamilton, Ontario 1988.

[35] Building and Housing Research Center (BHRC). last accessed 2021, http://smd.bhrc.ac.ir/Portal/en/Search/Waveforms. n.d.

[36] Rezaee Manesh M, Saffari H. Empirical equations for the prediction of the bracketed and uniform duration of earthquake ground motion using the Iran database. Soil Dyn Earthq Eng 2020;137:106306. https://doi.org/10.1016/j.soildyn.2020.106306.

[37] Heydari M, Mousavi M. The Comparison of Seismic Effects of Near-field and Far-field Earthquakes on Relative Displacement of Seven-storey Concrete Building with Shear Wall. Curr World Environ 2015;10:40–6. https://doi.org/10.12944/CWE.10.Special-Issue1.07.

[38] Bhandari M, Bharti SD, Shrimali MK, Datta TK. Seismic Fragility Analysis of Base-Isolated Building Frames Excited by Near- and Far-Field Earthquakes. J Perform Constr Facil 2019;33:04019029. https://doi.org/10.1061/(ASCE)CF.1943-5509.0001298.

[39] Wang G-Q, Zhou X-Y, Zhang P-Z, Igel H. Characteristics of amplitude and duration for near fault strong ground motion from the 1999 Chi-Chi, Taiwan Earthquake. Soil Dyn Earthq Eng 2002;22:73–96. https://doi.org/10.1016/S0267-7261(01)00047-1.

[40] Li S, Xie L. Progress and trend on near-field problems in civil engineering. Acta Seismol Sin 2007;20:105–14. https://doi.org/10.1007/s11589-007-0105-0.

[41] Yadav KK, Gupta VK. Near-fault fling-step ground motions: Characteristics and simulation. Soil Dyn Earthq Eng 2017;101:90–104. https://doi.org/10.1016/j.soildyn.2017.06.022.

[42] Moniri H. Evaluation of seismic performance of reinforced concrete (RC) buildings under near-field earthquakes. Int J Adv Struct Eng 2017;9:13–25. https://doi.org/10.1007/s40091-016-0145-6.

[43] Gorai S, Maity D. Seismic response of concrete gravity dams under near field and far field ground motions. Eng Struct 2019;196:109292. https://doi.org/10.1016/j.engstruct.2019.109292.

[44] Kaklamanos J, Baise LG, Boore DM. Estimating Unknown Input Parameters when Implementing the NGA Ground-Motion Prediction Equations in Engineering Practice. Earthq Spectra 2011;27:1219–35. https://doi.org/10.1193/1.3650372.

[45] Seismo Signal. Pavia, Italy: Seism soft Ltd. Retrieved from http://www.seism osoft .com/en/HomeP age.aspx. 2020.

[46] Riddell R, Garcia JE. Hysteretic energy spectrum and damage control. Earthq Eng Struct Dyn 2001;30:1791–816. https://doi.org/10.1002/eqe.93.

[47] Makris N, Black CJ. Evaluation of Peak Ground Velocity as a "Good" Intensity Measure for Near-Source Ground Motions. J Eng Mech 2004;130:1032–44. https://doi.org/10.1061/(ASCE)0733-9399(2004)130:9(1032).

[48] Akkar S, Özen Ö. Effect of peak ground velocity on deformation demands for SDOF systems. Earthq Eng Struct Dyn 2005;34:1551–71. https://doi.org/10.1002/eqe.492.

[49] Bianchini M, Diotallevi P, Baker JW. Prediction of inelastic structural response using an average of spectral accelerations. 10th Int. Conf. Struct. Saf. Reliab., vol. 1317, 2009.

[50] Kohrangi M, Kotha SR, Bazzurro P. Ground-motion models for average spectral acceleration in a period range: direct and indirect methods. Bull Earthq Eng 2018;16:45–65. https://doi.org/10.1007/s10518-017-0216-5.

[51] Alavi B, Krawinkler H. Effects of near-fault ground motions on frame structures. John A. Blume Earthquake Engineering Center Stanford; 2001.

[52] Chopra AK, Chintanapakdee C. Comparing response of SDF systems to near-fault and far-fault earthquake motions in the context of spectral regions. Earthq Eng Struct Dyn 2001;30:1769–89. https://doi.org/10.1002/eqe.92.

[53] Panella DS, Tornello ME, Frau CD. A simple and intuitive procedure to identify pulse-like ground motions. Soil Dyn Earthq Eng 2017;94:234–43. https://doi.org/10.1016/j.soildyn.2017.01.020.

[54] Travasarou T, Bray JD, Abrahamson NA. Empirical attenuation relationship for Arias Intensity. Earthq Eng Struct Dyn 2003;32:1133–55. https://doi.org/10.1002/eqe.270.

[55] Arias A. Measure of earthquake intensity. Massachusetts Inst. of Tech., Cambridge. Univ. of Chile, Santiago de Chile; 1970.

[56] Sarma SK, Yang KS. An evaluation of strong motion records and a new parameterA95. Earthq Eng Struct Dyn 1987;15:119–32. https://doi.org/10.1002/eqe.4290150109.

[57] Electrical Power Research Institute (EPRI). A criterion for determining exceedance of the operating basis earthquake. Report No. EPRI NP-5930, Palo Alto, CA. 1988.

[58] Campbell KW, Bozorgnia Y. A comparison of ground motion prediction equations for Arias intensity and cumulative absolute velocity developed using a consistent database and functional form. Earthq Spectra 2012;28:931–41.

[59] Malhotra PK. Cyclic-demand spectrum. Earthq Eng Struct Dyn 2002;31:1441–57. https://doi.org/10.1002/eqe.171.

[60] Hancock J, Bommer JJ. The effective number of cycles of earthquake ground motion. Earthq Eng Struct Dyn 2005;34:637–64. https://doi.org/10.1002/eqe.437.

[61] Housner GW. Spectrum intensities of strong-motion earthquakes 1952.